

Prospecting for the Surface Treatment of a Nickel-Aluminium Bronze Alloy Using the TIG Process

Bruna Larissa Tascheck^{1*} , Tiago Vieira da Cunha¹ 

¹ Universidade Federal de Santa Catarina – UFSC, Centro Tecnológico de Joinville – CTJ, Joinville, SC, Brasil.

How to cite: Tascheck BL, Cunha TV. Prospecting for the surface treatment of a nickel-aluminium bronze alloy using the TIG process. *Soldagem & Inspeção*. 2023;28:e2801. <https://doi.org/10.1590/0104-9224/SI28.01>

Abstract: In this study the TIG process was used to perform the surface treatment of Nickel-Aluminium Bronze alloy (C63280), the main material used in the industry for the manufacture of naval propellers. The process was applied in specimens obtained from a propeller blade at different current pulsation frequencies (2, 5, 6, 12 Hz and 30 kHz) and without pulsation. The treatments were submitted to microstructural and microhardness analysis, and the results were compared to the material without any treatment. As for the microstructural aspect, all treatments resulted in grain refining, as this aspect is more accentuated for the frequency of 6Hz. The analysis also revealed a lower volume of the α phase in all treatments, which was evidenced upon investigation of the microhardness, with dispersion of the β phase in all samples and the k phase in some samples. The results show a greater uniformity in the microhardness in the treated zone due to grain refining. However, when comparing the average microhardness with the microhardness of the reference material, a significant increase of the microhardness was reached only at the frequency of 6Hz.

Keywords: Nickel-Aluminium bronze alloy; Naval propellers; Surface treatment; TIG; Current pulsation.

1. Introduction

The propeller is the main propellant mechanism of many naval vessels. Its function is paramount for their performance. Therefore, a harmonious compromise between its requirements such as high efficiency, low probability of cavitation, noise, erosion, vibration, and low maintenance costs is required [1]. The combination of these qualities, associated with the large diameters a propeller can attain and the nature of which it is manufactured make it a component of high added value. As a result, surveys are constantly carried out to extend the useful life of these components (vessel propellers) that are so important to naval vessels.

The phenomenon of cavitation is undoubtedly the most common and, above all, the most harmful to vessel propellers, which occurs in flows at high speeds in a fluid, when the static pressure drops to a value less than the vapor pressure thereof. In this condition, steam bubbles arise that are charged to a region where if the pressure increases again, implosion occurs [2]. Due to the aggressive mode in which these vapor bubbles implode, the surface of the material is then attacked, thus degrading the blades constituting the propeller. As a way of resisting this attack, the material must possess characteristics that provide greater mechanical resistance. Thus, changing the microstructure of the material is a strategy normally approached as a way to provide the propeller more adequate properties in the attempt to prolong the exercise of its function [3-5]. In this context, the superficial treatments frequently found in the specialized literature indicate lasers as its main source of energy. As a result, several laser welding techniques have been developed in order to improve the materials, especially against cavitation erosion [6].

The American Bureau of Shipping [7] identifies Nickel-Bronze Aluminum Alloy (NAB) C63280 as being a material commonly employed in the manufacture of naval propellers. This is mainly due to the high resistance to corrosion and wear presented by this material. According to Hyatt et al. [8], a higher resistance to cavitation erosion is obtained by deposition on the NAB using the laser cladding technique (LC) using NAB itself as the addition material. Applying this technique, Hyatt et al. [8] obtained the alteration of the microstructure of the surface of large columnar grains for smaller ones, varying the contribution of heat in the material. However, it was observed the formation of the Widmanstätten α phase, characterized by Bell [9] due to its low corrosion resistance in the presence of sea water, making the technique not feasible for applications in propellers or other parts that operate underwater. In the case of the Widmanstätten phase, Cottam et al. [10] observed its presence by applying the technique of laser surface melting (LSM) welding in NAB. In addition, they also identified the presence of a lamellar precipitate (kIII), which is more susceptible to cavitation erosion and contributes to the low material cavitation performance. The same authors also analyzed the processing of the NAB alloy with the Laser Processed (LP) technique, but in this case they did not identify the presence of the kIII phase. However, the rate of cavitation erosion in materials treated by both techniques is very similar, since the microhardness analysis revealed that the samples processed by Laser Processed had a lower hardness. In this context, Tang et al. [3-5] using laser surface alloying (LSA) and

Received: 11 Nov., 2021; Accepted: 10 Nov., 2022.

E-mails: bruna.tascheck@t2f.ufsc.br (BLT), t.cunha@ufsc.br (TVC)



This is an Open Access article distributed under the terms of the [Creative Commons Attribution license](https://creativecommons.org/licenses/by-nc/4.0/), which permits unrestricted use, distribution, and reproduction in any medium, provided the original work is properly cited.

LSM in the surface treatment of Manganese-Nickel-Aluminum bronze alloy (MAB), a similar material and of the same application as NAB, obtained an increase in resistance to cavitation erosion in both cases. However, these treatments conferred greater brittleness to the material, as cavitation erosion tests revealed that the fragile fracture mode prevailed, with the material being broken in the weak triple junctions and grain boundaries.

The TIG welding process allows the use of several techniques, among them a very widespread one being the pulsation of the welding current. This technique has been used in the processing of various materials over the past years and its application has shown good results. The application of the pulsed TIG process is associated with several benefits in welding, namely in obtaining grain refining.

Mehdi et al. [11] compared the pulsed TIG and conventional TIG techniques in Ti-6Al-4V titanium alloy welding and observed a higher grain refining effect in the treated region of the samples obtained with the pulsed current, the effect being greater for higher pulsation frequencies of the welding current (1 to 5 Hz). On the other hand, when the microhardness of these samples was analyzed, the highest value obtained was for the frequency of 1Hz, while the sample submitted to the frequency of 5Hz presented the lowest values. This is due to the β -phase grain refinement, caused by the increase in pulse rate. Sundaresan et al. [12] emphasize the effects obtained with the pulsed technique when applying the TIG process with and without current pulsation in Ti-6Al-4V and Ti-6Al-2Sn-4Zr-2Mo titanium alloys. According to the authors, among the studied frequencies (2, 4, 6 and 8 Hz), the highest grain refining effect and the highest tensile strength were obtained specifically at the frequency of 6 Hz. Kishore Babu et al. [13] and Balasubramanian et al. [14] also carried out a similar study with titanium alloy Ti-6Al-4V, also indicating the pulsation frequency of the 6 Hz current as the one where the effects of pulsation become more evident and that, therefore, microstructural and mechanical properties are obtained. These results agree with those obtained by Padmanaban and Balasubramanian [15], which evaluated the effects of different pulsation frequencies of the current through the TIG process on the tensile strength of AZ31B magnesium alloy. This shows, therefore, that the effects obtained with the pulsation of the current are not exclusive to titanium alloys, but also possible to be obtained in other materials, including NAB.

In relation to the pulsation of the current in the TIG process, the most recent technique approached by the studies available in the literature has been the introduction of ultrasonic energy in arc welding by the pulsation of the current in frequencies above 20 kHz. The method of the ultrasonic excitation of the arc is a relatively recent resource, whose main purpose is to impart better mechanical properties to the weld bead. When dealing specifically with the microstructural aspect of the weld beads, researchers present as a result of the application of the mentioned technique metallurgical changes that are justified by the intense propagation of the ultrasonic energy in the material. According to Eskin and Eskin [16] this propagation thus causes the generation of cavitation inside the melting chamber. The collapse of the cavitation bubbles thus breaks down the crystals of the growing grains by positively altering the microstructure of the material. Another observed effect concerns the reduction of the gases and impurities present in the melting pool, thus improving the mechanical properties of the materials.

Applying the current pulsation technique in ultrasonic frequencies in the SiCp / 6061Al MMCs material, for the frequencies of 30 kHz, 50 kHz and 70 kHz, Lei et al. [17] observed a reduction in grain size, increased tensile strength, and increased penetration of weld beads. According to the authors, the best results were obtained with the lower frequencies of ultrasonic pulsation, since increasing frequency does not allow sufficient time for the complete development of cavitation, thus reducing the mechanical properties of the material. Similar results were obtained by Zhu et al. [18] when studying the effects of ultrasonic pulsation in MGH956 alloy for the frequency range of 30 to 80 kHz. According to their results it was not possible to establish a correlation between the microhardness values obtained and the frequencies used. However, with respect to tensile strength, the highest value obtained was for the sample produced at the frequency of 30kHz.

Despite the improvements obtained in NAB and in materials of similar nature, processed with techniques that use laser as the heat source, the relatively high cost of the equipment involved and the level of qualification of personnel required must be considered. In view of this, the use of processes that use the arc as a heat source is the most accessible alternative. Regarding this consideration, no reference was found in the literature addressing the use of the TIG process in NAB processing. Based on this, the present study aims to perform the surface treatment of NAB alloy, employing the TIG process with the pulsating current technique at different frequencies. This, in order to identify possible microstructural and mechanical changes that may be reflected in improvements in the resistance to corrosion and erosion by cavitation of the material.

2. Materials and Methods

The specimens were obtained from a propeller blade. Due to the complex geometry and thickness variations, the dimensions of the specimens were optimized in order to maximize the number of specimens. Thus, six specimens were obtained, initially obtained by a water-cooled cutting process in order to maintain their microstructural integrity and, afterwards, finishing with a machining process in order to give them the dimensions of 90 x 80 x 6 mm. The composition of the NAB alloy employed in the present work was determined by Atomic Absorption Spectrophotometry and Gravimetry to determine the Copper (Cu) content.

The Pulsed TIG process was used with the parameters shown in Table 1. As a reference, a non-pulsed test was also performed, using a constant current (CC-) with a value equal to the mean value used in the tests with pulsed current.

Table 1. Regulated welding parameters used in the tests.

Specimens	Welding speed [cm/min]	Base current (I _b) [A]	Peak current (I _p) [A]	Average calculated current [A]	Current pulse frequency [Hz]	Current pulse amplitude [A]
1	5	-	-	68	-	-
2	5	35	85	68	2.5	50
3	5	35	85	68	6.0	50
4	5	35	85	68	12.0	50
5	5	35	85	68	30000.0	50

In all tests pure argon was used as the shielding gas, with a flow rate of 10 l/min. The distance between electrode and piece (DEP) used was 3mm, with the EWTh-2 electrode having a diameter of 2.4mm. The tests involved casting a surface area of 30mm². In order to do so, a displacement system with two degrees of freedom was used, in which it was programmed to develop a rectangular trajectory. Thus, at the end of each section traversed in the X direction, the system displaced the welding torch 0.5 mm from the Y direction before performing the return movement at X direction. With this, it was possible to establish an approximate 0.25 mm overlap between the weld beads. After the tests were carried out, the specimens were cooled to room temperature.

The samples were obtained by means of the subdivision of the treated area of 30mm² of the specimens. These samples, together with an untreated sample of the material (MB - withdrawn directly from the propeller blade) were then cold embedded. Subsequently, they underwent a sanding process starting with the grit size 80 and then with the grades 120, 320, 600 and 1200, followed by polishing with diamond paste with granulometry of 3μ and 1μ, respectively. Finally, the samples were chemically attacked according to Cottam et al. [10] in a solution containing 5g FeCl₃ + 15ml HCl + 60ml ethanol for 3s.

The depth of the treated region (surface region of the specimens that were melted by the welding process) was analyzed in a stereoscope, and the values presented in the present study consist of the arithmetic average obtained from three measurements. For the micrographic analyses, an optical microscope model IM100i was used. For the purposes of identifying the observed phases, the images were compared with those obtained by the authors Marsico [19], Rodrigues et al. [20], and Cottam et al. [10]. The analysis of the volumetric fractions of the present phases was done with the aid of the software Digimet Plus 5G provided by MIP Systems from the images with the magnification of 200X. Furthermore, analyses were carried out of these images to determine the average grain size using the intercept method according to ASTM E 112.

Finally, Vickers microhardness tests were performed according to ASTM E384-11. The microhardness profile, composed of 20 indentations in each sample, was collected along the thickness of the specimen, starting at 0.5 mm from the surface of the samples. The load applied in the test was 200g (0.2 kgf) lasting 15s.

3. Results and Discussions

The analysis of the chemical composition, shown in Table 2, revealed that the material studied is a NAB alloy classified by the Unified Numbering System for Metals and Alloys (UNS) as the alloy C63280 [21].

Table 2. Composition in wt.% of as-received NAB.

Cu	Al	Fe	Ni	Mn
80.55	8.30	4.54	4.30	0.98

As can be seen, this alloy has 8.30% Al. Due to this percentage of Al, the phase χ is not present in this material. This phase has a low electrochemical potential and is therefore a preferential phase for corrosion in the presence of salt water. Thus, its absence is beneficial to the material as it does not reduce its mechanical resistance and corrosion [22].

The values of the welding current and arc voltage measured, and welding energy calculated are shown in Table 3. The Equation 1 was used to calculate the welding energy as a function of the sum of the product of the instantaneous welding current (I_i) and instantaneous arc voltage (U_i) measures in "n" points and as a function of the welding speed (Ws). It is possible to observe that the welding energy for all the tests was approximately equal. This allows, therefore, to disregarding possible effects related to the influence of the welding energy on the obtained results.

$$E = \frac{1}{n \cdot Ws} \sum_{i=0}^n U_i \cdot I_i \quad (1)$$

Table 3. Measured and calculated variables.

Specimens	Measured		Calculated	
	Current pulse frequency [Hz]	Average arc voltage [V]	Average welding current [A]	Welding Energy [J/mm]
1	-	12.4	69	1058
2	2.5	12.9	68	1084
3	6.0	12.0	68	1003
4	12.0	11.9	69	1001
5	30.000	12.5	69	1051

Figure 1 shows the mean penetration depth values of the treated region for each of the samples produced. The mean value of this depth for all the tests was approximately 2.5mm, which is compatible with those obtained by Cottam et al. [10] applying the LP technique. However, it is possible to notice significant variations (in the order of 40%) in this value, when considering the depths obtained in the tests with 6 and 12 Hz. This result can be related to the arc profile or process fusion efficiency obtained in these frequencies, and its possible influence in weld bead width. According to Ugla [23], the pulsation frequency is an important parameter of influence on the aspect ratios of bead width and depth of penetration. Its results show a significant reduction in the weld bead width obtained with a 6 Hz current pulsation frequency when compared to that obtained in constant current, in which it can be attributed to a more constricted arc due to current pulsation. Thus, since the welding torch displacement was the same in all tests, this would affect the overlapping indices between the weld beads. As a result, different energy inputs are locally delivered to the piece, thus affecting the depth of the treated region.

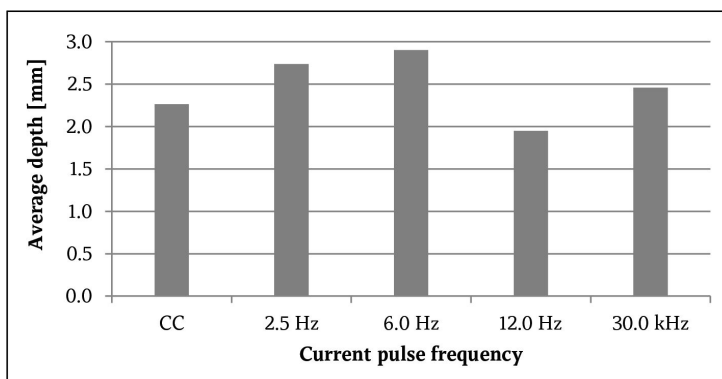


Figure 1. Average depth of treated region.

Figure 2 shows the microstructural aspect of the untreated sample of the material (MB) and the interface between the treated (ZT) and untreated (ZNT) regions. In these images a significant grain refining in the ZT is evident, relative to the material as received (MB sample shown in the Figure 3 - CC), as a result of the application of the surface treatment. The grain refining obtained is possibly a consequence of the heating process of the material, raising its temperature just above the melting temperature, at approximately 1070 °C, promoting, thus, the grain breakage and phase transformations, reconciled to a cooling at room temperature that prevented the growth of the grains. Also in these images, it is possible to identify variations in the depth of penetration of the treated region, accompanied by a very characteristic pattern of lines in the ZT region. A more detailed analysis of this region (Figure 3) shows a considerable variation in the grain sizes present in the ZT region, especially in samples treated with 2.5 and 6.0 Hz, which is a result of the overlap between the weld beads. Thus, it is believed that when the voltaic arc overlaps the previous bead, the heat input from the voltaic arc promotes the fragmentation of the growing crystals in the preceding bead. This reinforces, therefore, the effect that the thermal cycle imposed by the voltaic arc has on the microstructure of the material.

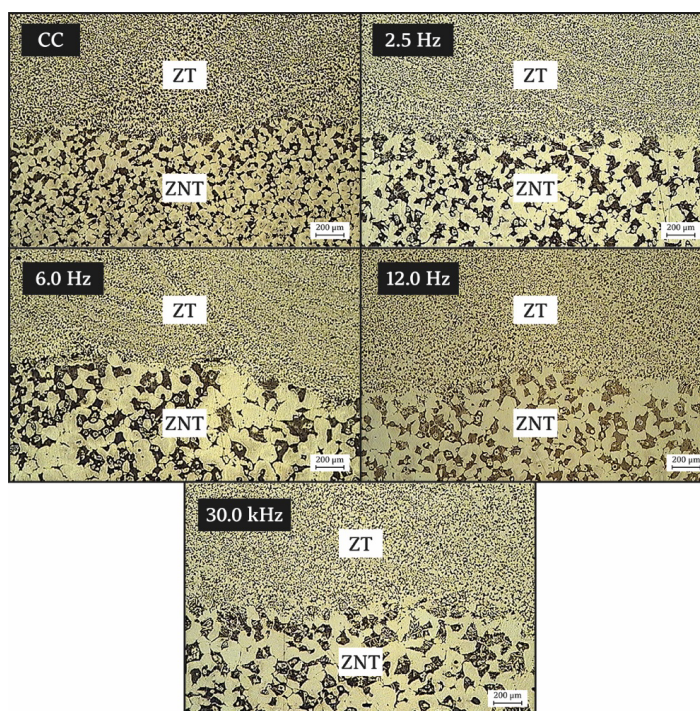


Figure 2. Micrographs of the interface region between ZT and ZNT.

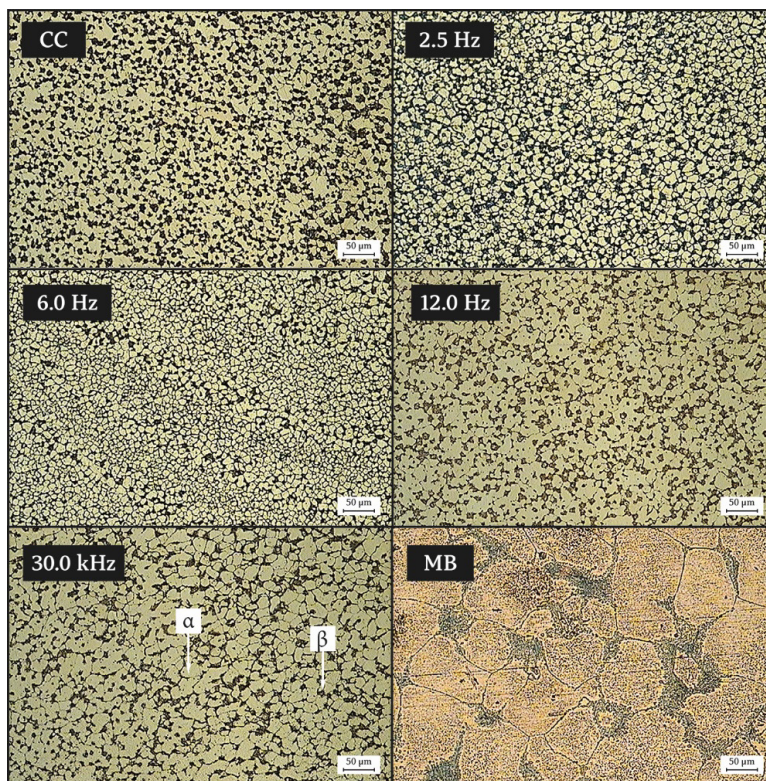


Figure 3. Micrographs of the ZT region.

By comparison with images present in works available in the literature, in Figure 3 (30.0 kHz) it is possible to identify phase α , rich in Cu, and phase β , composed of phases $\alpha + k$ [10]. As can be seen, the α phase is predominant in the microstructure, which is responsible for the ductility characteristic of the material. The β phase, due to its constitution, is a phase that naturally presents a higher hardness, thus contributing to increased resistance to erosion by cavitation. In order to identify a possible influence of the treatment employed in relation to the quantity of these phases, analysis of the volumetric fraction of the phases α and β was carried out. The result is shown in Figure 4. As can be seen, the base material (MB) is the one with the largest volume of the α -phase. However, the samples processed, including those without any current pulsation, had lower percentages of that phase. This was most accentuated for the samples produced with the 2.5Hz and 6Hz current pulse frequencies, which resulted in β phase percentages of about 40%. However, the volume of the α -phase present in these samples is still considerably higher than the volume of the β -phase. Thus, even with the percentage increase of about 70% of the β phase, the resulting proportion of these phases leads to obtaining a material with higher ductility and, consequently, a greater elongation, thus reducing the probability of the occurrence of fragile-fracture-type faults.

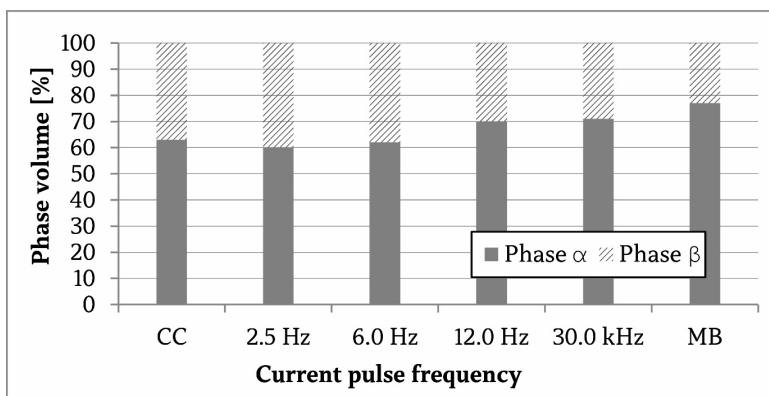


Figure 4. Volume of the α and β phases present in the samples.

The average grain size analysis, shown in Figure 5, shows that all treated samples obtained significant grain refining. Based on the standard deviation of the results, it can be stated that the refining achieved is very similar in all samples. This result

indicates that the thermal cycle to which the material was subjected during the treatment is the main factor attributable to the microstructural changes. This implies, therefore, that the use of current pulsation is not necessary. This is favorable from an economic and productive point of view, as the use of simpler equipment can be used while not relying on highly specialized knowledge in order to properly define the variables related to pulsed current. However, although not significant in relation to the other samples, the result obtained with the frequency of 6Hz presented the highest value of grain refining. This result agrees with Sundaresan et al. [12], which found in their investigation that the frequency of 6Hz is the most appropriate for grain refinement, as well as Reddy et al. [24], who also obtained optimal values of ultimate tensile strength of Al alloys in welded joints at 6Hz. According to Sundaresan et al. [12], the effect of the current pulsation on the solidification of the bead at very low frequencies is very small. On the other hand, at very high frequencies, the amplitude of vibration and temperature oscillation induced in the weld pool are reduced. Therefore, the effects are maximized at intermediate pulsation frequency.

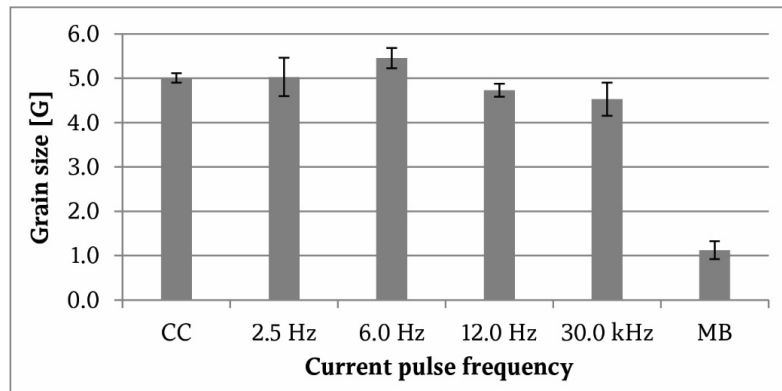


Figure 5. Average grain size of samples according to ASTM E 112-11.

An even more detailed analysis of the treated region (with 1000X magnification) revealed the existence of spherical intermetallic precipitates (Figure 6). By comparison with images present in the works of Rodrigues et al. [20] and Cottam et al. [10], it is assumed these precipitates are phase k (designation given by these authors). The intermetallic phases designated k (kI, kII, kIII, kIV) can be constituted of Fe₃Al, FeAl, or NiAl depending on the composition of the alloy. The identification of phase k present in the resulting microstructure is not within the scope of this work, being treated only as phase k. As explained by Marsico [19], these phases are derived from the higher concentrations of Ni and Fe introduced into the material to increase its mechanical strength. In this context, Ni increases corrosion resistance, while Fe acts as a grain refiner increasing tensile strength. Thus, the presence of both contributes to increasing the stability of the α phase and reduces the formation of the β phase.

It is possible to observe that in the samples obtained with pulsation frequencies of 2.5Hz, 6Hz and in constant current, a homogenous distribution of these precipitates (of smaller size) was obtained in the material. Already in the frequency of 12Hz and 30kHz, this phase is present in islands of great volume. The pulsed current applied in the TIG process promotes cyclic thermal energy variations on the weld pool. In this context, Garland [25] exemplifies that decreasing the pulse current allows the solid-liquid phase to advance toward the arc and become increasingly vulnerable to any perturbation in the shape of the arc, subsequently with the increase of pulse current, growth of the grains of the material is interrupted, thereby consequently reducing the cooling rate and promoting the refining of the grains. The thermal cycles used in the higher frequencies (12Hz and 30kHz) occur in short intervals, interrupting the solidification process of the material, thus preventing further refining of phase k and other phases for these frequencies. Due to its characteristics, Marsico [19] shows that the more refined and dispersed these precipitations are in the α phase, as in samples produced with 2.5Hz, 6.0Hz, and CC, the higher the corrosion resistance and the hardness of the material. On the other hand, when the k phase is concentrated in specific regions, the hardness of the material is basically defined by phase β , which is more dispersed in its microstructure with respect to phase k. According to Rodrigues et al. [20], this is one disadvantage of this condition as it imparts a lower corrosion resistance.

The Widmanstätten phase was not observed in any of the treated samples. It is assumed that the absence of this phase, characteristic of the alloy NAB when cooled rapidly [10], is due to the slow cooling occurred at room temperature. Another benefit provided by slow cooling was non-formation of the β' phase. This is called the martensitic phase due to its acicular shape, which gives the material a high hardness value. Thus, the use of a subsequent heat treatment in order to transform the β' phase to β is unnecessary. Furthermore, according to Zhang et al. [26], phase β' is anodic with respect to the matrix α , which reduces the corrosion resistance of NAB. In this context, the presence of the β phase as a result of the treatment carried out results in smaller variations in the hardness of the material, as can be observed in Figure 7.

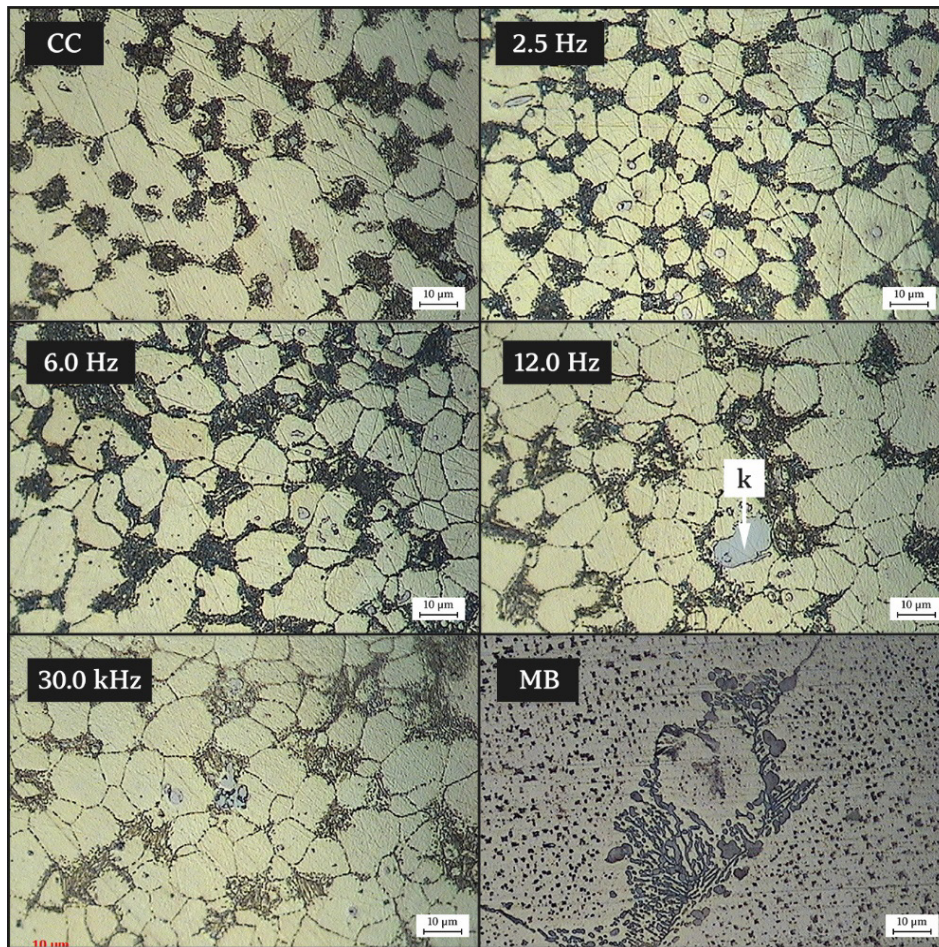


Figure 6. Micrographs of the ZT region.

In Figure 7 the microhardness profiles obtained at the interface between the ZT and ZNT regions are presented for all samples. It is observed that the microhardness values obtained in the ZT region show a significantly lower amplitude of variation than those obtained in the ZNT region. This result can be attributed to the fragmentation and dispersion of the phases β and k within the α phase. On the other hand, the dispersion of the results obtained in the ZNT can be justified by the larger grain size present in this region. Thus, the hardness peaks obtained represent the indentations performed on the β phases, whereas the points of lesser hardness represent the indentations performed on the α phase, as shown in Figure 8.

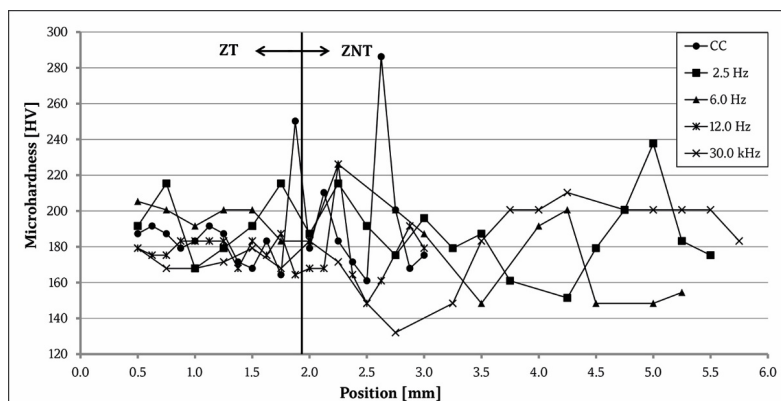


Figure 7. Microhardness profile obtained at the interface between the ZT and ZNT regions.

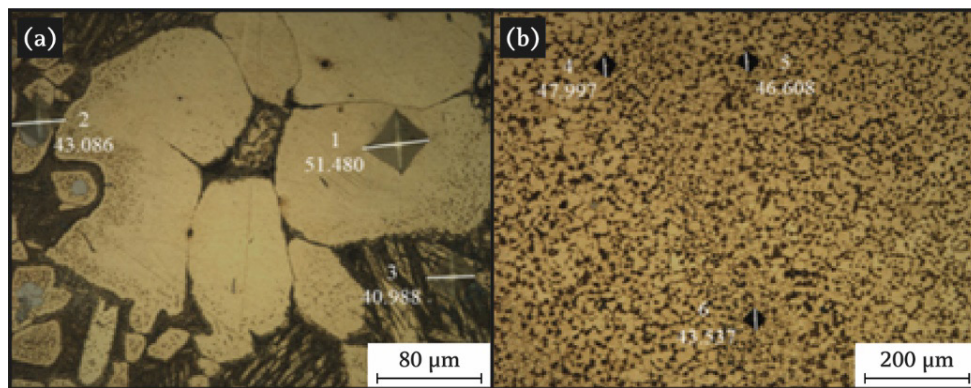


Figure 8. Indents carried out in the regions a) ZNT and b) ZT.

In the images of Figure 8 the location where three indentations were performed in each of the ZNT and ZT regions is shown. As can be observed, these indentations are located on different phases present in the ZNT. Phase α (indentation 1) has the lowest value of microhardness, approximately 139HV. Indentation 2 was performed on phase k , resulting in a microhardness value of about 200HV. The highest microhardness value was obtained for indentation 3, performed in a larger volume of the β phase, at a value of approximately 220HV. The indentations performed in the ZT region (Figure 8b) presented similar values. This result was already expected, considering that in this region the microstructure is more refined due to the treatment performed with the TIG arc. However, analyzing Figure 8b it is possible to observe that the indentation 6 was performed in a region of grains of smaller size (possibly due to overlap between the weld beads), resulting in a hardness value of 195HV. Indentations 4 and 5 are located in a coarser granulation region, resulting in lower hardness values, 160 and 170HV, respectively.

Figure 9 shows the mean value of microhardness obtained in the ZT region in the different samples. As expected, the highest microhardness value obtained for the sample was processed at the frequency of 6Hz (198HV), due to the higher grain refining obtained (Figure 5). This means a hardness increase of about 10% when considered the untreated material sample (MB), of which the mean value was 176HV.

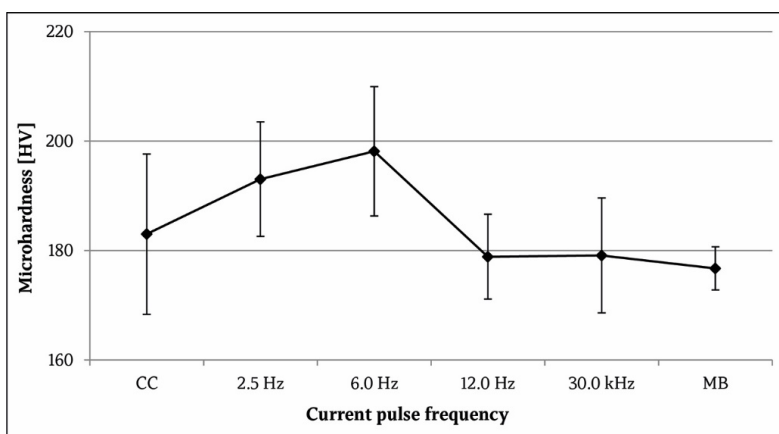


Figure 9. Mean value of microhardness obtained in the ZT region of the different samples.

The higher hardness observed in the ZT is derived from obtaining the most dispersed phases β and k on the α phase, an aspect that tends to increased resistance to erosion by cavitation. Furthermore, the α phase, which is responsible for the ductility characteristic of the material, is present in considerable volume in the ZT. This, together with the significant grain refining in the treated region, makes the surface treatment with the TIG process a promising technique for obtaining superior mechanical properties in the Nickel-Aluminium Bronze Alloy with a lower cost involved.

4. Conclusions

The microstructural and microhardness characteristics of NAB alloy submitted to the TIG process were analyzed and compared with untreated NAB. On that basis, the following conclusions were reached:

- Regarding the effects obtained with the application of the technique in relation to the resulting microstructure, it is concluded that all surface treatments achieved a visible level of grain refining. For the sample treated with the frequency of 6Hz, the greatest level of grain refining was obtained;
- The phases of Widmanstätten and β' were not observed, thus avoiding the problems arising from them;
- Dispersion of the β phase was observed in all samples and of phase k in samples produced with CC, 2.5Hz and 6.0Hz, providing higher values of microhardness for these samples;
- When it comes to microhardness, the application of the technique resulted in higher values of microhardness with respect to the CC sample for all the treatments performed, but in order to achieve a higher level of grain refining, the frequency of 6Hz provided a hardness increase of about 11%.

Authors' contributions

BLT: Conceptualization, data curation, formal analysis, investigation, methodology, validation, writing – original draft, writing – review & editing. TVC: Data curation, investigation, methodology, supervision, writing – original draft, writing – review & editing.

Acknowledgements

The authors are grateful to the Laboratory of Welding Technology (UFSC-Joinville) and the company IMC Welding for assistance with this research.

References

- [1] Naval Studies Board, National Research Council. Twenty-fourth symposium on naval hydrodynamics. Washington, DC: National Academies Press; 2003.
- [2] d'Agostino L, Salvetti MV. Fluid dynamics of cavitation and cavitating turbopumps. Wien: Springer Science & Business Media; 2008.
- [3] Tang CH, Cheng FT, Man HC. Laser surface alloying of a marine propeller bronze using aluminium powder. *Surface and Coatings Technology*. 2006;200(8):2602-2609. <http://dx.doi.org/10.1016/j.surfcoat.2004.12.021>.
- [4] Tang CH, Cheng FT, Man HC. Effect of laser surface melting on the corrosion and cavitation erosion behaviors of a manganese–nickel–aluminium bronze. *Materials Science and Engineering A*. 2004;373(1-2):195-203. <http://dx.doi.org/10.1016/j.msea.2004.01.016>.
- [5] Tang CH, Cheng FT, Man HC. Improvement in cavitation erosion resistance of a copper-based propeller alloy by laser surface melting. *Surface and Coatings Technology*. 2004;182(2-3):300-307. <http://dx.doi.org/10.1016/j.surfcoat.2003.08.048>.
- [6] Kwok CT, Man HC, Cheng FT, Lo KH. Developments in laser-based surface engineering processes: with particular reference to protection against cavitation erosion. *Surface and Coatings Technology*. 2016;291:189-204. <http://dx.doi.org/10.1016/j.surfcoat.2016.02.019>.
- [7] American Bureau of Shipping. Rules for survey after construction. Houston: ABS; 2009.
- [8] Hyatt CV, Magee KH, Betancourt T. The effect of heat input on the microstructure and properties of nickel aluminum bronze laser clad with a consumable of composition Cu-9.0 Al-4.6 Ni-3.9 Fe-1.2 Mn. *Metallurgical and Materials Transactions. A, Physical Metallurgy and Materials Science*. 1998;29(6):1677-1690. <http://dx.doi.org/10.1007/s11661-998-0090-5>.
- [9] Bell DE. Microstructural development and corrosion resistance of laser-welded nickel-aluminum bronze [masters dissertation]. Pennsylvania: Pennsylvania State University; 1994.
- [10] Cottam R, Luzin V, Moody H, Edwards D, Majumdar A, Wong YC, et al. The role of microstructural characteristics in the cavitation erosion behaviour of laser melted and laser processed Nickel–Aluminium Bronze. *Wear*. 2014;317(1-2):56-63. <http://dx.doi.org/10.1016/j.wear.2014.05.002>.
- [11] Mehdi B, Badji R, Ji V, Allili B, Bradai D, Deschaux-Beaume F, et al. Microstructure and residual stresses in Ti-6Al-4V alloy pulsed and unpulsed TIG welds. *Journal of Materials Processing Technology*. 2016;231:441-448. <http://dx.doi.org/10.1016/j.jmatprotec.2016.01.018>.
- [12] Sundaresan S, Janaki Ram GD, Madhusudhan Reddy G. Microstructural refinement of weld fusion zones in α – β titanium alloys using pulsed current welding. *Materials Science and Engineering A*. 1999;262(1-2):88-100. [http://dx.doi.org/10.1016/S0921-5093\(98\)01010-7](http://dx.doi.org/10.1016/S0921-5093(98)01010-7).
- [13] Kishore Babu N, Ganesh Sundara Raman S, Mythili R, Saroja S. Correlation of microstructure with mechanical properties of TIG weldments of Ti–6Al–4V made with and without current pulsing. *Materials Characterization*. 2007;58(7):581-587. <http://dx.doi.org/10.1016/j.matchar.2006.07.001>.
- [14] Balasubramanian V, Jayabalan V, Balasubramanian M. Effect of current pulsing on tensile properties of titanium alloy. *Materials & Design*. 2008;29(7):1459-1466. <http://dx.doi.org/10.1016/j.matdes.2007.07.007>.

- [15] Padmanaban G, Balasubramanian V. Optimization of pulsed current gas tungsten arc welding process parameters to attain maximum tensile strength in AZ31B magnesium alloy. *Transactions of Nonferrous Metals Society of China*. 2011;21(3):467-476. [http://dx.doi.org/10.1016/S1003-6326\(11\)60738-3](http://dx.doi.org/10.1016/S1003-6326(11)60738-3).
- [16] Eskin GI, Eskin DG. Production of natural and synthesized aluminum-based composite materials with the aid of ultrasonic (cavitation) treatment of the melt. *Ultrasonics Sonochemistry*. 2003;10(4-5):297-301. [http://dx.doi.org/10.1016/S1350-4177\(02\)00158-X](http://dx.doi.org/10.1016/S1350-4177(02)00158-X) PMID:12818397.
- [17] Lei Y, Wang Z, Chen X. Effect of arc-ultrasound on microstructures and mechanical properties of plasma arc welded joints of SiCp/Al MMCs. *Transactions of Nonferrous Metals Society of China*. 2011;21(2):272-277. [http://dx.doi.org/10.1016/S1003-6326\(11\)60709-7](http://dx.doi.org/10.1016/S1003-6326(11)60709-7).
- [18] Zhu Q, Lei Y, Wang Y, Huang W, Xiao B, Ye Y. Effects of arc-ultrasonic on pores distribution and tensile property in TIG welding joints of MGH956 alloy. *Fusion Engineering and Design*. 2014;89(12):2964-2970. <http://dx.doi.org/10.1016/j.fusengdes.2014.08.012>.
- [19] Marsico TA. *Microstructural development in cast and laser beam clad nickel aluminum bronze*. Pennsylvania: The Pennsylvania State University; 1996.
- [20] Rodrigues CA, Melo MDLNM, Paes LES. Caracterização de uma liga de bronze de alumínio submetida a diferentes tratamentos térmicos. *REM. Revista Escola de Minas*. 2012;65(3):343-348. <http://dx.doi.org/10.1590/S0370-44672012000300010>.
- [21] Kutz M. *Mechanical engineers' handbook: materials and engineering mechanics*. New Jersey: John Wiley & Sons; 2015.
- [22] Cook M, Davis E, Fentiman WP. Observations on the structure and properties of wrought copper-aluminium-nickel-iron alloys. *Journal of the Institute of Metals*. 1951;80:419-429.
- [23] Uglá AA. Enhancement of weld quality of AISI 304L austenitic stainless steel using a direct current pulsed TIG arc. *IOP Conference Series: Materials Science and Engineering*. 2018;433(1):012075. <http://dx.doi.org/10.1088/1757-899X/433/1/012075>.
- [24] Reddy GM, Gokhale AA, Rao KP. Optimisation of pulse frequency in pulsed current gas tungsten arc welding of aluminium–lithium alloy sheets. *Materials Science and Technology*. 1998;14(1):61-66. <http://dx.doi.org/10.1179/mst.1998.14.1.61>.
- [25] Garland JG. Weld pool solidification control. *Metal Construction*. 1974;4:121-127.
- [26] Zhang D, Ruiping CHEN, Zhang W, Zongqiang LUO, Yuanyuan LI. Effect of microstructure on the mechanical and corrosion behaviors of a hot-extruded nickel aluminum bronze. *Acta Metallurgica Sinica. English Letters*. 2010;23(2):113-120.